A&A 630, A146 (2019)
https://doi.org/10.1051/0004-6361/201936311


Astronomy & Astrophysics

# VEXAS: VISTA EXtension to Auxiliary Surveys

## Data Release 1. The southern Galactic hemisphere

C. Spiniello[1,2] and A. Agnello[3]

[1] INAF – Osservatorio Astronomico di Capodimonte, Salita Moiariello, 16, 80131 Napoli, Italy
e-mail: chiara.spiniello@inaf.it, chiara.spiniello@gmail.com
[2] European Southern Observatory, Karl-Schwarschild-Str. 2, 85748 Garching, Germany
[3] DARK, Niels Bohr Institute, Copenhagen University, Lyngbyvej 2, 2100 Copenhagen, Denmark

Received 14 July 2019 / Accepted 29 August 2019

**ABSTRACT**

*Context.* We present the first public data release of the VISTA EXtension to Auxiliary Surveys (VEXAS), comprising nine cross-matched multi-wavelength photometric catalogues where each object has a match in at least two surveys.
*Aims.* Our aim is to provide spatial coverage that is as uniform as possible in the multi-wavelength sky and to provide the astronomical community with reference magnitudes and colours for various scientific uses: object classification (e.g. quasars, galaxies, and stars; high-$z$ galaxies, white dwarfs); photometric redshifts of large galaxy samples; searches of exotic objects (e.g. extremely red objects and lensed quasars).
*Methods.* We cross-matched the wide-field VISTA catalogues (the VISTA Hemisphere Survey and the VISTA Kilo Degree Infrared Galaxy Survey) with the AllWISE mid-infrared Survey, requiring a match within 10″. We have further matched this table with X-ray and radio data (ROSAT, XMM, SUMSS). We also performed a second cross-match between VISTA and AllWISE, with a smaller matching radius (3″), including WISE magnitudes. We then cross-matched this resulting table ($\approx 138 \times 10^6$ objects) with three photometric wide-sky optical deep surveys (DES, SkyMapper, PanSTARRS). We finally included matches to objects with spectroscopic follow-up by the SDSS and 6dFGS.
*Results.* To demonstrate the power of all-sky multi-wavelength cross-match tables, we show two examples of scientific applications of VEXAS, in particular using the publicly released tables to discover strong gravitational lenses (beyond the reach of previous searches) and to build a statistically large sample of extremely red objects.
*Conclusions.* The VEXAS catalogue is currently the widest and deepest public optical-to-IR photometric and spectroscopic database in the southern hemisphere.

**Key words.** catalogs – surveys – virtual observatory tools

## 1. Introduction

Wide-field Sky surveys have become a fundamental tool for observational cosmology, for example to explore the large-scale structure and the role of dark matter and dark energy in the evolution of the Universe (e.g. the Kilo Degree Survey, KiDS, via weak lensing, Kuijken et al. 2015; Hildebrandt et al. 2017; ATLAS, Shanks et al. 2015; the Dark Energy Survey, DES, Dark Energy Survey Collaboration 2016) or the discovery of primordial quasars (out to the re-ionisation epoch, Venemans et al. 2013; Carnall et al. 2015; Reed et al. 2015; Bañados et al. 2016; Chehade et al. 2018), as well as for extragalactic astrophysics, e.g. the formation and evolution of galaxies, including the Milky Way, or the distribution of dark matter around galaxies (e.g. the Sloan Digital Sky Survey, SDSS, Abolfathi et al. 2018; The Two Micron All Sky Survey, 2MASS, Skrutskie et al. 2006; The Cosmic Evolution Survey, Scoville et al. 2007; The *Gaia* Mission, Gaia Collaboration 2016; The Galaxy And Mass Assembly, GAMA, Driver et al. 2011; Liske et al. 2015).

Over the last decade, astronomical surveys provided new insights into the physics of objects on all scales from giants early-type galaxies (ETGs) to faint and compact stellar systems, and at all distances from the structure and dynamics of our own galaxy to high-redshift quasars. Tracing the mass assembly of the big structures in our Universe, mapping the evolution of galaxy size–mass relation, detecting and studying the intracluster light components, understanding the transient phenomena and the time-domain in the Universe, and studying early cosmic times are only few of the astrophysical and cosmological questions that have been tackled by wide-field sky surveys.

Given the value of wide and deep photometric databases, calibrated and cross-matched tables with homogeneous spatial and wavelength coverage are fundamental. This is indeed the purpose of the VISTA EXtension to Auxiliary Surveys (VEXAS) project, which we present here.

In this first data release, covering the southern Galactic hemisphere (SGH), we cross-matched the two main extragalactic surveys on the Visible and Infrared Survey Telescope for Astronomy (VISTA, Emerson et al. 2006), with many of the most successful wide-sky photometric surveys in the optical (the Dark Energy Survey, DES, Abbott et al. 2018; the Panoramic Survey Telescope & Rapid Response System DR1, PanSTARRS1, Chambers et al. 2016; and SkyMapper Southern Sky Survey, SM, Wolf et al. 2018), in the infrared (the Wide-Infrared Survey Explorer, WISE, Wright et al. 2010), in the X-ray (ROSAT All Sky Survey, Boller et al. 2014, 2016; The *XMM-Newton* Serendipitous Survey, Watson et al. 2001), and in the radio domain (SUMSS, Bock et al. 1999). The core requirement is

a reliable photometry in more than one band. This condition, together with the detection in at least two surveys (via cross-match), should minimise if not completely eliminate the number of spurious detections in the final catalogues. Finally, we also identify all the objects retrieved by the VISTA catalogues that have a spectroscopic redshift estimate from the Sloan Digital Sky Survey (SDSS, DR14, Abolfathi et al. 2018) and/or from the 6dF Galaxy Survey (6dFGS, Jones et al. 2004). All the resulting tables are validated and publicly released through the ESO Phase 3[1].

The paper is organised as follows. In Sect. 2 we provide a brief description of the VISTA Surveys (VHS and VIKING), which are the starting points of the matches, and of the criteria leading to our VEXAS final table of 198 608 360 objects in the SGH. In Sects. 3 and 4 we introduce the infrared and optical public surveys and the multi-wavelength cross-match. For each cross-match we provide the total number of retrieved objects and the main characteristics of the final table. In Sect. 5 we focus on the spectroscopic cross-matches, also giving the final relative number of matched objects. In Sect. 6 we describe the matches with surveys covering larger wavelength bands, namely X-ray and radio. In Sect. 7 we provide two examples of interesting scientific cases where the VEXAS tables are clearly helpful: the identification of extremely red objects, and the search for strong gravitationally lensed quasars. Finally, we conclude in Sect. 8 and discuss possible developments for future data releases.

We always keep the native magnitude system of each survey unless a direct comparison is required between magnitudes given in different systems[2].

## 2. The VISTA Surveys

The Visible and Infrared Survey Telescope for Astronomy (VISTA; Emerson et al. 2006), hosted by the Paranal ESO Observatory and working at near-infrared (NIR) wavelengths, has a primary mirror of 4.1 m and was conceived to map the sky systematically in a survey manner. VISTA was conceived and developed by a consortium of 18 universities in the United Kingdom and most of the observing time was allocated by the European Southern Observatory (ESO) to six big public surveys[3].

For the purposes of this paper (i.e. a homogeneous and wide database for multi-wavelength studies) we focus on two VISTA Public Surveys with the largest footprints: the VISTA Hemisphere Survey (VHS, McMahon et al. 2013) and the VISTA Kilo Degree Infrared Galaxy Survey (VIKING, Sutherland 2012). The two surveys share the same reduction and processing. Astrometric and photometric calibrations are based on 2MASS (Skrutskie et al. 2006) stars: a set of colour equations is used to predict VISTA native magnitudes from the observed 2MASS $J, H, Ks$ colours (González-Fernández et al. 2018).

### 2.1. The VISTA Hemisphere Survey

The VISTA Hemisphere Survey (VHS, McMahon et al. 2013) covers the SGH to ≈30 times deeper limits than 2MASS in at least two near-IR bands ($J$ and $Ks$). With the advent of different optical surveys covering some areas of the southern sky, VHS provides complementary data to the $grizY$ broad-band photometry from DES (Abbott et al. 2018) in the south Galactic cap (SGC), and $ugriz$ from the VST-ATLAS survey (Shanks et al. 2015). The target depth (in Vega magnitudes) is $J = 20.6$, $H = 19.8$, $Ks = 18.5$ from 120 s integrations on the DES overlap, and somewhat shallower ($J = 20.2$, $Ks = 18.1$; 60 s per band) on the VST-ATLAS overlap.

### 2.2. The VISTA-Kilo-Degree Infrared Galaxy Survey

The VISTA-Kilo-Degree Infrared Galaxy Survey (VIKING, Sutherland 2012; Edge et al. 2013) covers 1500 square degrees overlapping the Kilo Degree Survey (KiDS, Kuijken et al. 2015) for the optical counterpart, ensuring a uniform coverage on ∼1350 deg$^2$ with intermediate depth in nine bands ($grizYJHKs$, with limiting magnitude $J = 21$ in the Vega system), enabling accurate photometric redshift measurements for weak-lensing studies (Hildebrandt et al. 2017). The science goals of the KiDS and VIKING include the following: the characterisation of galaxy clusters up to $z \sim 1$ (Maturi et al. 2019), the search for high-$z$ objects (Venemans et al. 2015) and new strong gravitational lenses (Spiniello et al. 2018; Petrillo et al. 2019; Khramtsov et al. 2019), and the study of galaxy structural parameters and stellar masses for a statistically large sample of galaxies (Roy et al. 2018).

The sky coverage is at high Galactic latitudes, and includes two main stripes of ∼70 × 10° each: one in the SGC near declination (Dec) ∼ −30 deg, and one near Dec ∼ 0 deg in the north Galactic cap (NGC). By design, the VIKING and VHS footprints are complementary (see Fig. 2).

### 2.3. Querying the VISTA Surveys

We queried VIKING and the VHS-DR6 from the VISTA Science Archive website[4] directly. We note that the VHS-DR6 does not match the latest release from the ESO archive, as visible from Fig. 2.

To ensure that only objects with reliable photometry in at least one band are retrieved, we imposed the following criteria on the Petrosian magnitudes and their uncertainties:

$$(\Delta Ks < 0.3 \text{ and } 8 < Ks) \quad \text{or}$$
$$(\Delta H < 0.3 \text{ and } 8 < H) \quad \text{or}$$
$$(\Delta J < 0.3 \text{ and } 8 < J) \tag{1}$$

Moreover, for this VEXAS-DR1 we only consider objects below the Galactic plane, $b < -20$. This is the area where wide-field weak-lensing cosmological experiments overlap; it covers a hemisphere with narrower previous coverage, and also includes the well-studied Stripe-82 area of the SDSS. Comparable operations at $b > 20$ are planned for the second release of VEXAS.

Given the TAP limitations on the maximum file size and maximum number of objects per query, we had to split VHS into several declination slices. We show the slices in Fig. 1 and report the number of objects retrieved for each slice in Table 1. The whole VIKING-DR3 could instead be retrieved with a single ADQL (Astronomical Data Query Language) job.

For the VEXAS-DR1, both the VIKING and VHS queries included a `JOIN` command to the cross-neighbour AllWISE table, provided by the VISTA Science Archive[5] (VSA,

[1] https://www.eso.org/sci/observing/phase3.html. While processing the phase 3 documentation and format, we released the table via a temporary repository (here).

[2] When comparing magnitudes from different surveys, we adopt the conversions given here http://casu.ast.cam.ac.uk/surveys-projects/wfcam/technical/filter-set

[3] VISTA is an in-kind contribution to ESO as part of the UK accession agreement.

[4] http://horus.roe.ac.uk/vsa/

[5] http://horus.roe.ac.uk/vsa/www/vsa_browser.html

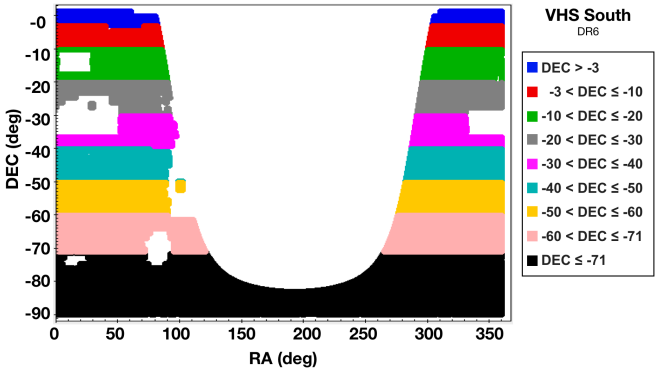


**Fig. 1.** Final coverage (in right, right ascension, RA, and declination, Dec) of the products retrieved from the VHS DR6 for this release of VEXAS. The colours indicate different Dec slices that we built to overcome the TAP limitations on size and/or entries. The number of objects for each slice is given in Table 1.

**Table 1.** Number of objects in each declination slice, plotted in Fig. 1.

| Declination | Objects |
|---|---|
| $+3 < \mathrm{Dec} \leq -3$ | 9 439 341 |
| $-3 < \mathrm{Dec} \leq -10$ | 15 829 509 |
| $-10 < \mathrm{Dec} \leq -20$ | 23 321 667 |
| $-20 < \mathrm{Dec} \leq -30$ | 21 954 249 |
| $-30 < \mathrm{Dec} \leq -40$ | 20 453 315 |
| $-40 < \mathrm{Dec} \leq -50$ | 27 090 911 |
| $-50 < \mathrm{Dec} \leq -60$ | 25 319 673 |
| $-60 < \mathrm{Dec} \leq -71$ | 22 406 811 |
| $-71 < \mathrm{Dec}$ | 21 839 924 |

Cross et al. 2012), containing all the AllWISE sources within 10.0″ of each VHS source. No further requirements were made on the AllWISE entries, except that they exist.

Finally, after querying VIKING and VHS separately, we concatenated the tables using the TOOL FOR OPERATIONS ON CATALOGUES AND TABLES (TOPCAT, Taylor 2005)[6]. The final number of objects retrieved with these criteria is 198 608 360, of which 187 655 440 from VHS+AllWISE and 10 952 920 from VIKING+AllWISE. We list in Table 2 the number of objects retrieved for each of the cross-matches we carried out starting from the VEXAS table described above.

## 3. Infrared photometric cross-matches: VEXAS-AllWISE

The Wide-Infrared Survey Explorer (WISE, Wright et al. 2010) NASA mission provided all-sky astrometry and photometry in four mid-infrared bandpasses centred on 3.4 $\mu$m (hereafter W1), 4.6 $\mu$m (hereafter W2), 12 $\mu$m (hereafter W3) and 22 $\mu$m (hereafter W4).

The NeoWISE project (Mainzer et al. 2011) extended the original WISE mission after its cryogenic phase. Combining these two complete sky coverage epochs, the AllWISE data have enhanced photometric sensitivity and accuracy, and improved astrometric precision compared to the previous WISE All-Sky Data Release. The WISE science goals include the search and characterisation of the very luminous red galaxies, the search for nearby coolest stars, and the study of the nature of asteroids and comets.

The AllWISE Source Catalogue (Cutri et al. 2013) used for this VEXAS release includes ≈747 million objects over the whole sky, with median angular resolution of 6.1, 6.4, 6.5, and 12.0 arcsec respectively for the four bands.

In addition to the match with the cross-neighbour AllWISE table directly from the VISTA Science Archive, we perform a further match with a smaller matching radius of 3″, retrieving also the WISE magnitudes and their associated errors. The choice of 3″ is a compromise between the resolution of WISE (≈6″) and spurious cross-matches between different sources with ghosts and artefacts. The VEXAS-AllWISE3 table ("3" indicates the matching radius) comprises 126 372 293 objects with photometry in at least one VISTA band and in the WISE bands ($W1$ to $W4$, with errors). For completeness, we also provide the 2MASS (Skrutskie et al. 2006) IDs and magnitudes in $JHKs$ bands whenever they are available.

Throughout the paper, and for all the further cross-matches, we use the VEXAS-AllWISE3 table as a starting point unless otherwise specified. The `JOIN` cross-match with AllWISE3 ensures a large wavelength final baseline for our catalogues, and at the same time limits (or completely eliminates) spurious detections, given that each object has at least three independent matches from three different surveys.

The luminosity functions of VISTA-AllWISE objects are shown in Fig. 3. For the sake of comparison, we also show the 2MASS luminosity functions in the same ranges. This release of VISTA-AllWISE objects extends the 2MASS depth by 2−3 mag. This is consistent with the target depths of the VHS and VIKING. The main limitation at the faint end is given by the requirement that the magnitude errors be ≤0.3 mag. The luminosity functions corresponding to ≤0.1 mag errors follow the 2MASS luminosity function more closely.

The role of AllWISE seems sub-dominant in this regime, compared to that of the upper limit on VISTA magnitude errors. If the constraints on magnitude errors were loosened, then the depth of AllWISE would be the main limitation, but the VISTA pipeline magnitudes would still be unreliable. Therefore, fainter samples from the VHS and VIKING would need model-based forced photometry from auxiliary catalogues.

**Table 2.** Number of objects in VEXAS, from VISTA and subsequent cross-matches.

| Cat. table | Objects |
|---|---|
| VEXAS | 198 608 360 |
| VEXAS-AllWISE3 | 126 372 293 |
| VEXAS-DESW | 37 615 619 |
| VEXAS-PS1W | 24 693 386 |
| VEXAS-SMW | 20 331 041 |
| VEXAS-EXTRAGAL | 5 742 300 |
| VEXAS-SPEC | 347 076 |
| VEXAS-21 cm | 77 338 |
| VEXAS-X-ray | 3049 |

**Notes.** The optical cross-matched tables are built from the VEXAS-AllWISE3 (matching radius of 3″). The spectroscopic table uses SDSS and 6dFGS and it is also matched with VEXAS-AllWISE3. The X-ray table used the 2RX+AllWISE and XMM+AllWISE tables by Salvato et al. (2018) (see Sect. 6 for more details) and the 21 cm table is obtained from SUMSS. In these two cases the match with AllWISE is within a 10″ matching radius, given the poorer resolution of X-ray and 21 cm surveys.

[6] http://www.star.bris.ac.uk/~mbt/topcat/

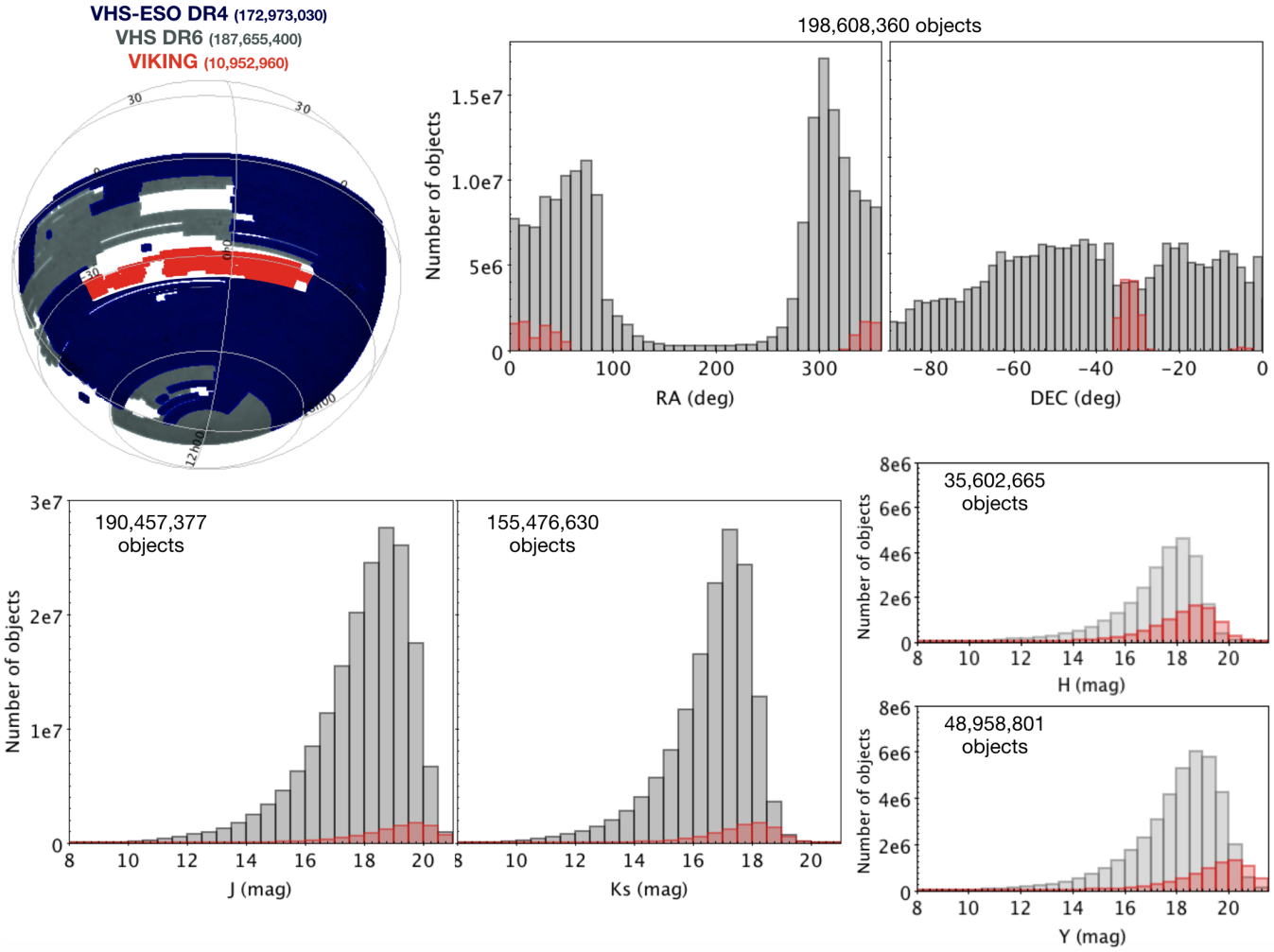


**Fig. 2.** *Left*: sky view of the VISTA footprint (VHS in grey and VIKING in red) compared to the VHS-ESO DR4 (blue). *Right*: histograms of RA and Dec for the VISTA Surveys that we used for this VEXAS-DR1. The total number of objects in the catalogue is shown above each histogram. *Bottom*: distribution of $Ks$, $J$, $H$, and $Y$ magnitudes of the input VISTA table, with number of objects within the magnitude ranges of Eq. (1) given in the top left corner of each panel. The VSH has a very broad coverage in $J$ and $Ks$, but only observed $H$ and $Y$ in a few fields.

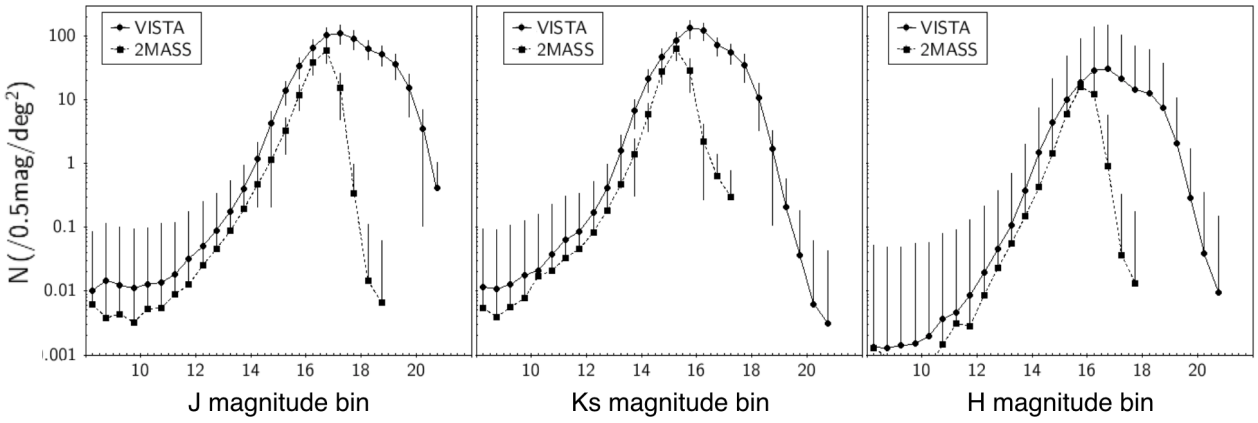


**Fig. 3.** Luminosity functions in $J$ (*left*), $Ks$ (*middle*), and $H$ (*right*) bands from VISTA (circles, continuous line) and 2MASS (squared, dotted lines) in bins of 0.5 mag (in the Vega system).

## 4. Public optical surveys and optical cross-matches

In order to maximise wavelength coverage and reach a wide mapping of the southern sky, we selected three of the most successful wide-field, multi-band optical photometric surveys: the Dark Energy Survey (DES, Abbott et al. 2018), the Panoramic Survey Telescope and Rapid Response System 1 (PanSTARRS1, hereafter PS1, Chambers et al. 2016) and the SkyMapper Southern Sky Survey (Wolf et al. 2018).

For this work we retrieved the latest public releases (DES-DR1, PS1-DR2, SkyMapper-DR1) and cross-matched them onto the final VISTA table of Sect. 2. All matches were performed

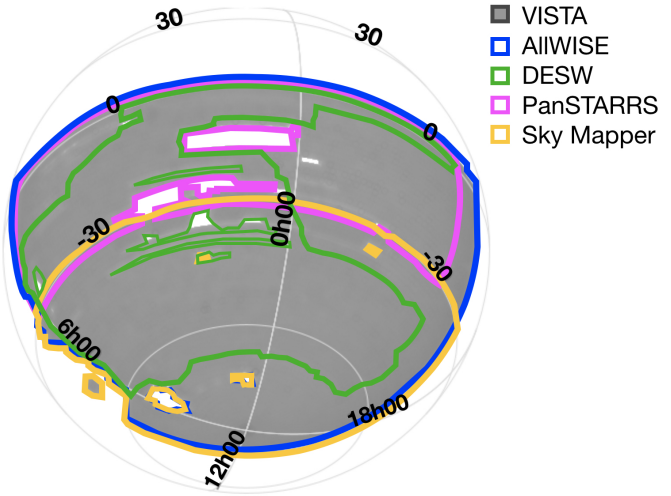


**Fig. 4.** Sky view of the VEXAS plus optical table footprints, plotted over the VISTA catalogue footprint (grey).

with TOPCAT, using the "Join – Pair Match". Unless otherwise specified, we used the "Sky" Matching algorithm with a maximum tolerance of 3″.

The tables are described in the following sub-sections. Their sky footprint is shown in Fig. 4, also including the coverage of the VISTA and AllWISE catalogues. The tables are publicly released and are available for the scientific community through the ESO Phase-3 interface[7].

### 4.1. VEXAS-DESW

The DES covered 5000 deg$^2$ of the southern sky using the 570-megapixel Dark Energy Camera (DECam, Diehl 2012), mounted on the Blanco 4 m telescope at Cerro Tololo Inter-American Observatory. It provides photometry in *grizY* filters, reaching limiting magnitudes ($10\sigma$: $g_{\rm lim}$ = 24.45, $r_{\rm lim}$ = 24.30, $i_{\rm lim}$ = 23.50, $z_{\rm lim}$ = 22.90, $Y_{\rm lim}$ = 21.70) faint enough to detect about 100 million stars, 300 million galaxies, $\approx 10^5$ galaxy clusters, and some $z > 6$ quasars (Dark Energy Survey Collaboration 2016).

The VEXAS-DESW final table comprises 37 615 619 objects with *grizY* photometry from DES, near-IR from VISTA, and mid-IR from WISE. In particular, all the objects have a match in AllWISE, with at least one measured WISE magnitude, at least one detection among the *grizY* bands and one among the VEXAS *YJHKs* bands. Finally, 1 971 448 objects have reliable photometry (within the $10\sigma$ limiting magnitudes) in all optical and infrared bands plus *W*1 and *W*2[8].

For each entry and for each survey (VISTA and DES), we provide the right ascension (RA) and declination (Dec)[9], the source ID, and the optical and infrared magnitudes with corresponding errors (*grizy* from DES, *YJHKs* from VISTA). For each entry in the table we also give the separation, computed by TOPCAT, between the centroid in DES and the centroid in VISTA. In addition, we provide the *W*1 and *W*2 magnitudes from AllWISE, the Galactic dust extinction value measured from the Schlegel maps (Schlegel et al. 1998), plus a number of columns that quantify the extendedness of the source, in particular PSTAR, the probability that the source is a star, from VISTA imaging and `spread_model_i`, `spreaderr_model_i`, and `wavg_mag_psf_i` from DES. The `spread` indicator values and errors are used by the DES collaboration to identify galaxies (as detailed by Vikram et al. 2015). Alternatively, the difference `wavg_mag_psf-wavg_mag_auto`, also provided, between PSF-like and isophotal magnitudes, can be used to separate point-like and extended sources.

We note that the magnitudes in the tables are provided in their native system of reference (AB for DES, Vega for VISTA and WISE). However, in Fig. 5 (upper panel), in order to provide a direct comparison between the *Y*-band magnitudes measured from DES and those measured for the same band from VISTA, we translate the latter into the AB system, using the following simple equation: $Y_{\rm AB} = Y_{\rm Vega} + 0.643$[10]. A fair agreement can be found for 99% of the ≈1.4 M objects for which the *Y* band is measured in the two surveys. Nevertheless a few differences can be seen at the brightest and faintest end. In particular, the VISTA magnitudes appear to be systematically brighter for ≈18 000 objects ($Y_{\rm VISTA} - Y_{\rm DES} < -1$), of which ≈15 000 are bright stars ($Y_{\rm VISTA} < 13$, PSTAR > 0.85), however, with a large error on the $Y_{\rm VISTA}$ magnitude (>0.5 mag). In the figure we plot the objects with $\delta Y_{\rm VISTA} < 0.5$ and $\delta Y_{\rm VISTA} < 0.5$ in purple, and the objects with larger error values in one or both surveys in grey. It is clear that considering only objects with small magnitude errors alleviates this disagreement, but does not resolve it. As a direct visual inspection of 1000 randomly selected objects confirmed, they are mostly saturated sources. We can then ascribe the *Y*-band mismatch to artificially faint magnitudes estimated by the DES pipeline on saturated objects.

### 4.2. VEXAS-PS1W

The Pan-STARRS1 (PS1) comprises the first two data releases of images taken with the PS1 1.8 m telescope at the Haleakala Observatories in Hawaii, equipped with a 1.4 gigapixel camera Kaiser et al. (2002), which covered the entire sky north of Dec = −30 deg. Its *grizy* filter set is comparable to that of the DES, although it is somewhat shallower ($5\sigma$: $g_{\rm lim} = 23.3$, $r_{\rm lim} = 23.2$, $i_{\rm lim} = 23.1$, $z_{\rm lim} = 22.3$, $Y_{\rm lim} = 21.4$).

The VEXAS-PS1W final table comprises 24 693 386 objects with optical photometry from PS1 and infrared photometry from VISTA. As in the previous case, all the objects have at least one magnitude entry among the *grizY* bands and at least one among the VEXAS *YJHKs* bands. Of these, 2 328 832 have photometry (within the $5\sigma$ limiting magnitudes) measured in all nine bands.

For VEXAS-PS1W we provide source ID, coordinates, and magnitudes (with associated errors and in the original reference system) for both surveys, the separation between the centroids, plus the probability of being a star and the Galactic dust extinction value from VISTA. For PanSTARRS DR1 we give Petrosian magnitudes in each of the optical bands and also the PSF *i*-band magnitude, its associated errors, and the stellarity likelihood. Moreover, as already done for VEXAS-DESW, all the entries have a match in AllWISE and thus we provide the *W*1 and *W*2 magnitudes in the Vega magnitude system.

The lower panel of Fig. 5 shows the AB *Y*-band comparison between PanSTARRS and VISTA. Also in this case, the major-

[7] For the time being, while making the tables Phase-3 compliant, we release them in the common FITS format via a temporary repository (here).

[8] The bottleneck is the *Y* band from VISTA, which has only been measured for 2 402 713 sources.

[9] Coordinates are given in the original format: radiants for VISTA and degrees for all the other surveys.

[10] We used standard Vega-to-AB conversions, summarised here: `http://www.astronomy.ohio-state.edu/~martini/usefuldata.html`

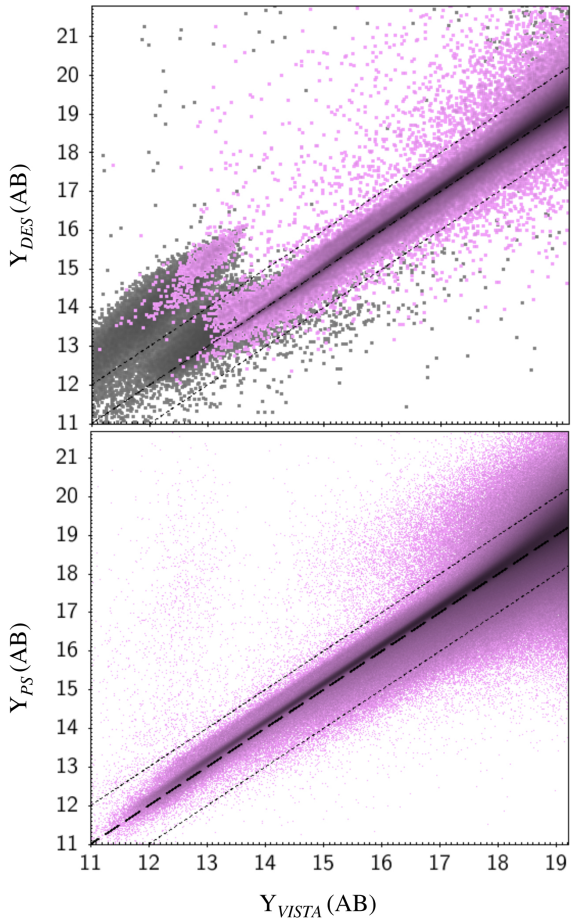


**Fig. 5.** Direct comparison between $Y$-band magnitudes from optical and infrared surveys, in the AB reference system, for objects with reliable photometry in an overlap of VISTA and DES/PanSTARRS. The thick dashed lines follow $Y_{\rm PS/DES} = Y_{\rm VISTA}$, and the dotted lines delimit offsets of one magnitude, enclosing >95% of the sources. A small systematic difference can also be attributed to the slightly different filters used in the different surveys. The comparison between DES and VISTA magnitude (*upper panel*) shows ≈15 000 bright saturated objects with $Y_{\rm DES} > Y_{\rm VISTA} + 1$. This is less apparent in PS1, due to its smaller primary mirror and hence fewer saturation issues. The grey (resp. magenta) objects have $Y_{\rm VISTA}$ magnitude errors larger (resp. smaller) than 0.5 mag.

ity of the objects (96%) have $-1 < Y_{\rm VISTA} - Y_{\rm PA} < 1$, among sources with a trustworthy $Y$-band magnitude value (≈8000 objects, within the survey nominal limiting magnitude). The scatter becomes larger at magnitudes fainter than $Y > 17$, but a fair agreement is found between the two measurements. We note a small systematic difference with $Y_{\rm PA}$ of ∼0.2 mag fainter than $Y_{\rm VISTA}$. This is mostly driven by the different shape of the $y_P$ and $Y$ filters used in PS1 (Tonry et al. 2012a) and VISTA.

Due to its smaller primary mirror (≈1.8 m versus ≈4 m), PS1 is less affected than DES by the saturation issues described in the previous section and shown in the upper panel of the figure.

### 4.3. VEXAS-SMW

The Australian SkyMapper Southern Sky Survey[11] produces a homogeneous multi-band coverage of the southern sky, similar to that provided by the SDSS in the northern sky. The first data release covers an area of ≈17 000 deg$^2$ in six pass-bands (*uvgriz*) with point-source completeness limits in AB magnitudes of 17.75, 17.5, 18, 18, 17.75, and 17.5 for $u$, $v$, $g$, $r$, $i$, and $z$, respectively.

The cross-match between VISTA and Sky Mapper produces 20 331 041 objects; however, only 82 052 objects have measured photometry in all nine bands (*ugrizYJHKs*). The $H$ band from VISTA and the $u$ band from SM are the two least covered bands with ≈3.2 and ≈3.8 objects, respectively.

In the VEXAS-SMW final table we again provide coordinates and magnitudes for the two surveys, and the WISE ($W1$, $W2$) magnitudes. Two values for the Galactic dust extinction, calculated with the same maps (Schlegel et al. 1998), one for each survey, are provided. The difference between the two values is that VISTA uses the correction given in Bonifacio et al. (2000), which reduces the extinction value in regions of high extinction (i.e. $E(B-V) > 0.1$). Finally, in addition to the `PSTAR` stellarity from VISTA, we also provide the value `class_star` for Sky Matter. In principle, both values should quantify the likelihood of an object being an unresolved source. However they depend on the model that has been fitted to the data (in a given detection band) and also on the depth and image quality of the survey. A comparison between these two values for bright objects in the $i$ band (46 832 sources with $i < 15$ in the AB system, i.e. the peak of the $i$-band magnitude histogram), shows a fair agreement between `PSTAR` and `class_star` for 46 046 high-confidence stars. Among the remaining objects, 519 are classified as secure stars in SM (`class_star` > 0.99) but have very low `PSTAR`, and 8 objects have instead `PSTAR` > 0.95 but `class_star` < 0.4. Finally, 150 sources have `PSTAR` < 0.075 but `class_star` > 0.3. Using both stellarity indicators may help in classifying objects with extended morphology and appreciable colour gradients (e.g. quasars with bright host galaxies).

### 4.4. VEXAS-EXTRAGAL

As an ancillary by-product, we also produced a table of 5 742 300 objects with extragalactic colours in the VISTA footprint. We do so by requiring

$$W1 - W2 > 0.2 + \sqrt{\delta W1^2 + \delta W2^2} \quad (2)$$

on the WISE magnitudes (in the Vega system). This colour cut excludes most stellar objects, which have $W1-W2 \approx 0$. It generalises the exponential cut-offs proposed by Assef et al. (2013) to isolate AGN candidates, which had a more demanding threshold at $W1 - W2 > 0.7$ and were incomplete with respect to quasars at redshifts $z \gtrsim 2$. Our colour cut also retains most galaxies at $z \lesssim 2$ (which have $W1 - W2 \approx 0.35$). We note that we consider only the first two WISE bands since the sensitivity in $W3$ and $W4$ is significantly impacted by Earth-shine noise.

A fraction of contaminants include brown dwarfs and white dwarfs with an IR excess, which can be further skimmed if optical and NIR magnitudes from ground-based surveys are used. In general, more refined separations of galaxies, stars, and quasars can be performed if multi-band coverage is available (e.g. through optical-to-NIR colours). However, this is currently possible only for a part of the SGH.

For the VEXAS-EXTRAGAL table, we provide coordinates and magnitudes for the VISTA and AllWISE surveys, the match and the magnitudes for 2MASS (when available), the stellarity index (PSTAR), and the Galactic dust extinction values.

[11] Led by the Research School of Astronomy and Astrophysics at the Australian National University, in collaboration with seven Australian universities and the Australian Astronomical Observatory.

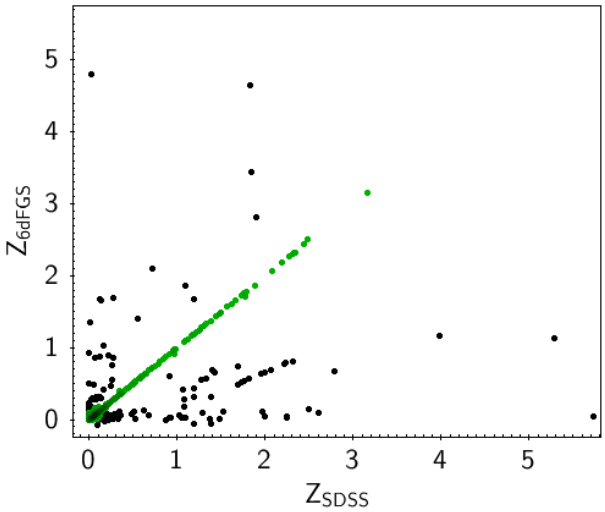


**Fig. 6.** Comparison of the redshifts computed from 6dfGS and these computed from SDSS for the common sample of 2834 objects. A good agreement is found for the 2709 green points that lie on the one-to-one line; for ∼5% of the sample (black points), the two surveys report very different redshift estimates for the same object.

## 5. Spectroscopic optical cross-matches

In multi-band object classification and discovery, the lack of spectroscopic information is a common issue. This holds especially in the SGH, where (at present) spectroscopic surveys are affected by depth, footprint, and preselection. However, part of the existing spectroscopic surveys do overlap with our VEXAS footprint. For this reason, we performed a spectroscopic cross-match between the final VISTA table and two of the most used all-sky spectroscopic surveys, the SDSS DR14 (Abolfathi et al. 2018) and the 6dFGS DR3 (Jones et al. 2004, 2009).

From the two surveys we only retrieved objects with a secure spectroscopic redshift measurement, using the "quality" keyword for 6dFGS (i.e. only objects with `qual=3` and `qual=4`, corresponding to 110 256 and 136 304 objects) and the error on the SDSS redshift value ($z_{\rm err} < 0.01$, 4 716 522 objects).

The cross-match produced 56 768 entries for 6dFGS and 347 076 for SDSS, of which 2834 objects have a double common match. These objects, with one or more spectroscopic classifications are contained in the table VEXAS-SPEC.fits, which is released as an ancillary product of the VEXAS DR1. The 2855 systems with a double match allow us to directly compare the redshift estimates that the two surveys provide on the same objects, as displayed in Fig. 6. For ∼95% of the sample with a double spectroscopic match, the two surveys agree well on the measured redshifts (green points, ∼96.5%). However for the remaining ∼4.5% of the matches, SDSS and 6dFGS strongly disagree on the redshift inference. There can be multiple reasons for the disagreement: blends of multiple objects in the same (slightly offset) fibre diameter, overcorrection of telluric absorption, splicing of the red and blue fibre spectra, and catastrophic failures in the pipelines for emission-line or absorption-line redshifts. For example, this problems leads to degenerate solutions for quasars at $z_{\rm s} \approx 0.77$ and $z_{\rm s} \approx 2.2$ in the low signal-to-noise regime.

## 6. Other wavelength cross-matches

To further extend the wavelength coverage of VEXAS, we also performed a cross-match with surveys in the radio and X-ray domain. In this case as well we required the existence of a match in the AllWISE catalogue for each object in order to eliminate spurious detections. However, we note that, given the poorer resolution of the matched surveys at these wavelengths, we kept the WISE matching radius to 10″ rather than restricting it to 3″ (as done in the optical).

In the radio domain, we retrieved 21 cm detection data from the Sydney University Molonglo Sky Survey (SUMSS, Bock et al. 1999), and performed the matches with ALLWISE and VISTA ourselves. For the X-rays, instead, we directly retrieved the catalogues presented by Salvato et al. (2018), hereafter S18, who performed a match of sources from the ROSAT all-sky survey (RASS, Boller et al. 2014, 2016) and the *XMM-Newton* with the AllWISE Source Catalogue taking into account magnitudes and number densities of the sources. In fact, given the large uncertainties in the positional errors of ROSAT/2RXS and XMM (see Fig. 1 in S18), they avoided making a too simplistic cross-match using coordinates only, and identified counterparts using a Bayesian approach and a prior defined using $W1$ and $W2$ from AllWISE (see also Dwelly et al. 2017 for the construction of the prior).

After cross-matching with VISTA, we obtained ≈37 000 objects with a match in another wavelength. Of these, 139 objects have a match in both X-ray and 21 cm catalogues, 3044 have a match in X-ray (1937 from 2RXS+AllWISE and 1147 from XMM+AllWISE), and 34192 have a 21 cm match. In the following we describe the cross-match procedures at higher and lower frequencies providing a brief description of the resulting tables, which are publicly available from VEXAS DR1.

### 6.1. VEXAS-XRAYs

We cross-matched VISTA with two among the most successful X-ray all-sky surveys in the 0.1−2.4 keV band: the ROSAT and the *XMM-Newton* Surveys.

The ROSAT all-sky survey (RASS) was the first observation of the whole sky in the 0.1−2.4 keV band (Truemper 1982). The RASS bright source catalogue (Voges et al. 1999), containing 18806 sources, and the RASS faint source catalogue (Voges et al. 2000) containing 105 924 sources down to a detection likelihood limit of 6.5 were joined together in the ROSAT 1RXS catalogue (Boller et al. 2014), which was then finally reprocessed in Boller et al. (2016) (2RXS) with a new improved detection algorithm that significantly reduced the number of spurious sources.

The ESA X-ray Multi-Mirror Mission (*XMM-Newton*), launched on December 10th 1999, is the second cornerstore of the Horizon 2000 Science Programme of the European Space Agency's (ESA). The most recent catalogue, derived from data acquired during slews between pointed observations, covers 84% per cent of the sky (DR 2.0, 2017 March 14).

As already specified, we used the catalogues of S18, who performed a maximum likelihood match of sources from 2RXS and *XMM-Newton* with the AllWISE Source Catalogue. The total number of entries listed in the S18 catalogue for 2RXS+AllWISE is 132 254. Of these, 5926 have been flagged as uncertain detections and have therefore been excluded from our catalogue. For the match of XMM with AllWISE S18 found instead 19 141 matches. We then cross-matched these with the VISTA final table finding 1937 common detections for 2RXS+AllWISE and 1147 for XMM+AllWISE. The objects in common between 2RXS+AllWISE and XMM+AllWISE are 40, thus yielding 3044 unique sources with an X-ray. These sources are reported in the publicly released VEXAS-XRAYs table. For

each entry in the table we list the coordinates for VISTA (in radiants), coordinates for AllWISE and for the parent X-ray survey (in degrees), infrared magnitudes with corresponding errors and X-ray fluxes, the separation between the centroids of the different surveys, the Galactic dust extinction values, and the stellarity likelihood from VISTA.

### 6.2. VEXAS-21 cm

The Sydney University Molonglo Sky Survey (SUMSS, Bock et al. 1999; Mauch et al. 2003) is a radio imaging survey of the southern sky (Dec $< -30$ deg), covering 8100 deg$^2$ at 843 MHz with images with resolution of $43'' \times 43''$ cosec(Dec), rms noise level of about 1 mJy beam$^{-1}$ and a limiting peak brightness between 6 mJy beam$^{-1}$ and 10 mJy beam$^{-1}$. The final catalogue is complete to 8 mJy at Dec $\leq -50$ deg, and to 18 mJy at Dec $> -50$ deg. Positions in the catalogue are accurate to within $2''$ for sources with peak brightness $\geq$20 mJy beam$^{-1}$, and are always better than $10''$. The internal flux density scale is accurate to within 3%.

We queried the SUMSS catalogue table directly[12], and cross-matched it locally with our VEXAS-AllWISE3 by seeking the closest source within a $10''$ matching radius. This yielded 77 338 radio sources with a match in VISTA and AllWISE, which we report and release in the table VEXAS-21 cm.

## 7. Scientific cases

In the following sections we describe few scientific applications using the VEXAS tables to search for peculiar and rare objects on the sky, such as strong gravitationally lensed quasars or extremely red objects.

### 7.1. Extremely red objects

Extremely red objects (EROs) are massive high-redshift galaxies that have been identified in the infrared and whose colours are so red ($R-K > 5$ or $I-K > 4$, Vega system) that they are not found in surveys that select galaxies at visual wavelengths.

The first identification of EROs goes back to the first time that a deep survey of the 2 $\mu$m sky was carried out. Elston et al. (1988) reported the discovery of a new population of extended objects that occupy a region of the infrared colour–magnitude diagram that is separate from the locus of normal galaxies. In particular, they identified a group of galaxies with $K$ magnitudes of $\approx$17–18 and $R - K \geq 5$. The authors suggested that these objects may be high-redshift galaxies ($z > 6$) undergoing a luminous star-forming phase, or weakly evolved ETGs at $z \sim 1$–1.5. Since the late 1980s a great deal of effort has been devoted to surveying the infrared sky and many more EROs have been found (McCarthy et al. 1992; Thompson et al. 1999; Daddi et al. 2000).

The red colours of EROs are consistent with two classes of galaxies: (I) old passive galaxies at $z \sim 1$ with a large K-correction and (II) high-redshift star-forming galaxies or heavily dust-reddened AGN. Observations indeed suggest that both of these classes of objects populate the EROs class: a few objects were spectroscopically confirmed to be dynamically relaxed and passively evolving ETGs at $z \geq 1$, (pEROs, e.g. Stiavelli et al. 1999; Kong et al. 2006), but many others were detected in the sub-mm, thus identified as high-redshift starbursts reddened by strong dust extinction and characterised by high star formation rates (sfEROs, e.g. Andreani et al. 2000). We found pEROs to be the most massive ($M \geq 10^{11.5}\, M_\odot$; Saracco et al. 2005) and oldest (age $> 1$ Gyr; Cassata et al. 2008) galaxies at $z > 1$. In addition, the pEROs show strong clustering that is comparable to that of local massive ellipticals (e.g. Daddi et al. 2000; Roche et al. 2002; Brown et al. 2005; Shin et al. 2017). This strongly suggests that pEROs could be the progenitors of local massive ellipticals and that they can work as powerful tools to study the redshift evolution of the most massive galaxies in the local universe, and thus to test our current cosmological galaxy formation models (e.g. Gonzalez-Perez et al. 2011). The relative contribution of the two classes of objects to the ERO population is still unknown, thus it is of great importance to build a statistically large sample of candidates to enlarge the ERO population and constrain number counts and density, especially for pEROs, with high precision.

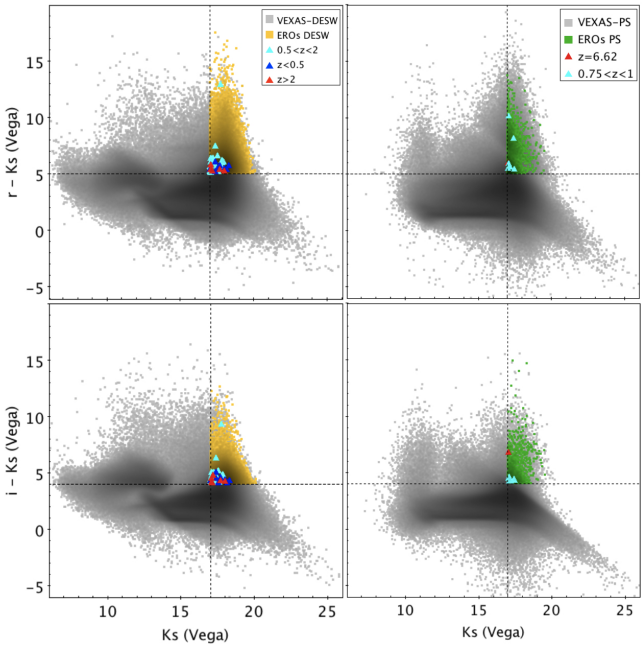


**Fig. 7.** Extremely red object candidates selected from the VEXAS-DESW catalogue (*left*, yellow) and from the VEXAS-PS catalogue (*right*, green) using the magnitude–colour thresholds defined in the text, highlighted in the plots with dotted lines. Triangles are the spectroscopically confirmed objects from the VEXAS-Spectroscopy table (59 in total).

Thanks to our cross-matched tables, we can now build a catalogue of ERO candidates and also put some constraints on the relative number of pEROs and sfEROs, performing a match with the VEXAS spectroscopic table. Following previous studies in the literature, we selected objects with

$$Ks \geq 17,\ Ks - i > 4,\ Ks - r > 5. \quad (3)$$

We applied these selection criteria to both the VEXAS-DESW and the VEXAS-PS final tables, finding a total of 1 010 205 EROs candidates (8758 from PS, 1 001 498 from DESW, and 51 in common)[13]. Then by cross-matching this table with the VEXAS spectroscopic table we also found 59 objects with a spectroscopic redshift and a secure classification. Among these objects, 26 are classified as QSOs and 7 have redshift $z > 2$,

[12] Available through the CDS portal, table `VIII/81B/sumss212`.

[13] The table "EROs-candidates.fits" is released as ancillary product of the VEXAS DR1.

while the remaining 33 are classified as GALAXY and have $0.19 < z < 1.64$.

Figure 7 shows the candidates from the two surveys in the colour–magnitude plots used for the selection. The spectroscopic objects are highlighted as triangles, colour-coded by their redshifts, as explained in the caption.

### 7.2. Astrometric offsets and lensed quasars

The astrometric consistency of sources across different catalogues can be used to identify close blends of multiple objects. One application is the detection of gravitational lenses, which are often blended in ground-based catalogue surveys due to their typical image separations and survey image quality.

In particular, strongly lensed quasars (QSOs) are rare objects that require a close alignment between a quasar and a massive galaxy. According to the estimations of Oguri & Marshall (2010), this happens once in $\sim 10^4$–$10^3$ times (see Agnello & Spiniello 2019, for revised estimates). The most successful ways to look for lensed QSOs are based on multi-colour preselection of QSOs and galaxies from wide-field surveys, followed by morphological criteria to isolate the rare cases of veritable lenses. For the first step, as largely demonstrated from previous work (and recalled in Sect. 7.3 below), a wide wavelength baseline is crucial in order to properly disentangle high-$z$ quasars from stars and galaxies (e.g. from blue optical bands to the mid-infrared). Thus, a homogeneous multi-wavelength coverage on the whole SGH. like VEXAS is ideal for this purpose. For the second step we use the very basic assumption that if the deflector and quasar images contribute differently in different bands, this should result in a centroid offsets of the same object among different surveys. To this end, in previous works (Spiniello et al. 2018; Agnello & Spiniello 2019) we developed the *BaROQuES* scripts[14] and we apply them here to the VEXAS-EXTRAGAL table where, thanks to the WISE colour cuts, we selected extragalactic objects, thereby eliminating the most stellar contaminants. The BaROQuES consider *field-corrected* offsets: for each object the astrometric offsets between different survey catalogues are computed in patches of $0.5 \times 0.5\,\mathrm{deg}^2$ around it, and their average is subtracted to the offset on the central object. This is done in order to remove any systematics from atmospheric differential refraction across surveys with different waveband coverage.

When DES (resp. SkyMapper) is combined with VISTA, ≈5% of the objects have field-corrected offsets above 0.26″ (resp. 0.4″). The threshold is comparable to the optical survey pixel size, but it also depends on the survey depth, which contributes to the astrometric accuracy on ground-based astrometry. In particular, for the DES, the sample can be further reduced (from ≈5% to ≈3%) if a magnitude-dependent cut is used for objects fainter than $i \approx 21$. Approximately half of the known lenses in the VEXAS-DES footprint have field-corrected offsets above the threshold, the other half being systems with larger separations and with bright ($i \lesssim 19$) catalogue magnitudes. Figure 8 displays some of the previously unknown gravitational lens candidates identified this way. Magnitude-dependent offset cuts are currently not relevant for SkyMapper, due to its rather larger pixel size and shallower limiting magnitudes.

Since different surveys are used to find close blends, the final sample selection can be affected by the limitations of each contributing survey. Figure 9 shows histograms of $i$-band, $JHKs$, and WISE magnitudes (and a stellarity indicator) for a subsample of BaROQuES in the DES and SkyMapper footprints, through different cuts. The samples are mostly unaffected by simple extragalactic colour cuts ($J - Ks > 0.85$, $i - W1 > 2.25$) or by a WISE colour cut. The main limiting aspect is the depth of the parent surveys; the depth of SkyMapper dominates the preselection, whereas for DES the main limitation is from the depth of WISE.

[14] Blue and Red Offsets of Quasars and Extragalactic Sources, available upon request, https://github.com/aagnello

### 7.3. Known lenses in VEXAS

Thanks to VEXAS, we can also better characterise the population of already known lenses to facilitate future searches. We assembled a table with 277 lenses collected by the CASTLES Project database (Muñoz et al. 1998), the SDSS Quasar Lens Search (SQLS, Inada et al. 2012), or recently discovered by us (Agnello et al. 2015, 2018a,b; Spiniello et al. 2019a,b) and other groups (e.g. Ostrovski et al. 2018; Anguita et al. 2018; Lemon et al. 2018). Among these lenses, 69 are in the VEXAS footprint, 48 are present in VEXAS-DESW, 26 in VEXAS-PS, 25 in VEXAS-SM, and 65 also have a match in AllWISE.

Figure 10 shows colour–magnitude or colour–colour plots of these known lenses in VEXAS. The known lenses typically span regions outside the stellar loci, and are generally characterised as extragalactic objects. While most have quasar-like hybrid colours, this is also a by-product of preselection in the older campaigns that identified them.

### 7.4. Galactic and solar system science

Most of the discussion above is centred on extragalactic applications. However, exploitation of our VEXAS catalogues is not limited to extragalactic science. For example, one aim of the NeoWISE mission was to identify near-Earth objects and asteroids (Mainzer et al. 2011). High proper-motion white dwarfs were among the first results by PanSTARRS1 (Tonry et al. 2012b). The disc and halo of the Milky Way have been mapped with dwarf and giant stars through 2MASS and optical data, also at regions of high Galactic latitude (e.g. Majewski et al. 2003; Bochanski et al. 2007; Gilmore et al. 2012; Carnero Rosell et al. 2019). Still in the south, various faint streams and Milky Way satellites have been discovered in the DES footprint (see e.g. Drlica-Wagner et al. 2015; Shipp et al. 2018).

As also shown by our Table 2, out of ≈138 million objects in the VISTA+AllWISE footprint, only ≈6 million have extragalactic WISE colours. The increased depth and coverage of VEXAS with respect to 2MASS and previous releases of the VHS should therefore allow for extensions of Galactic and solar system studies towards fainter magnitudes and with extended multi-band coverage.

## 8. Conclusions and future releases

In this paper we presented the first data release of VEXAS: the VISTA EXtension to Auxiliary Surveys (VEXAS DR1). We built the largest and most homogeneous multi-wavelength cross-matched photometric catalogue covering the southern hemisphere and containing only high-confidence objects with a match in at least two different surveys. In particular, we have performed the following actions:

– We used infrared multi-band photometry from the two wide-sky main VISTA Surveys, VHS (McMahon et al. 2013) and VIKING (Sutherland 2012) to build the VEXAS input table,

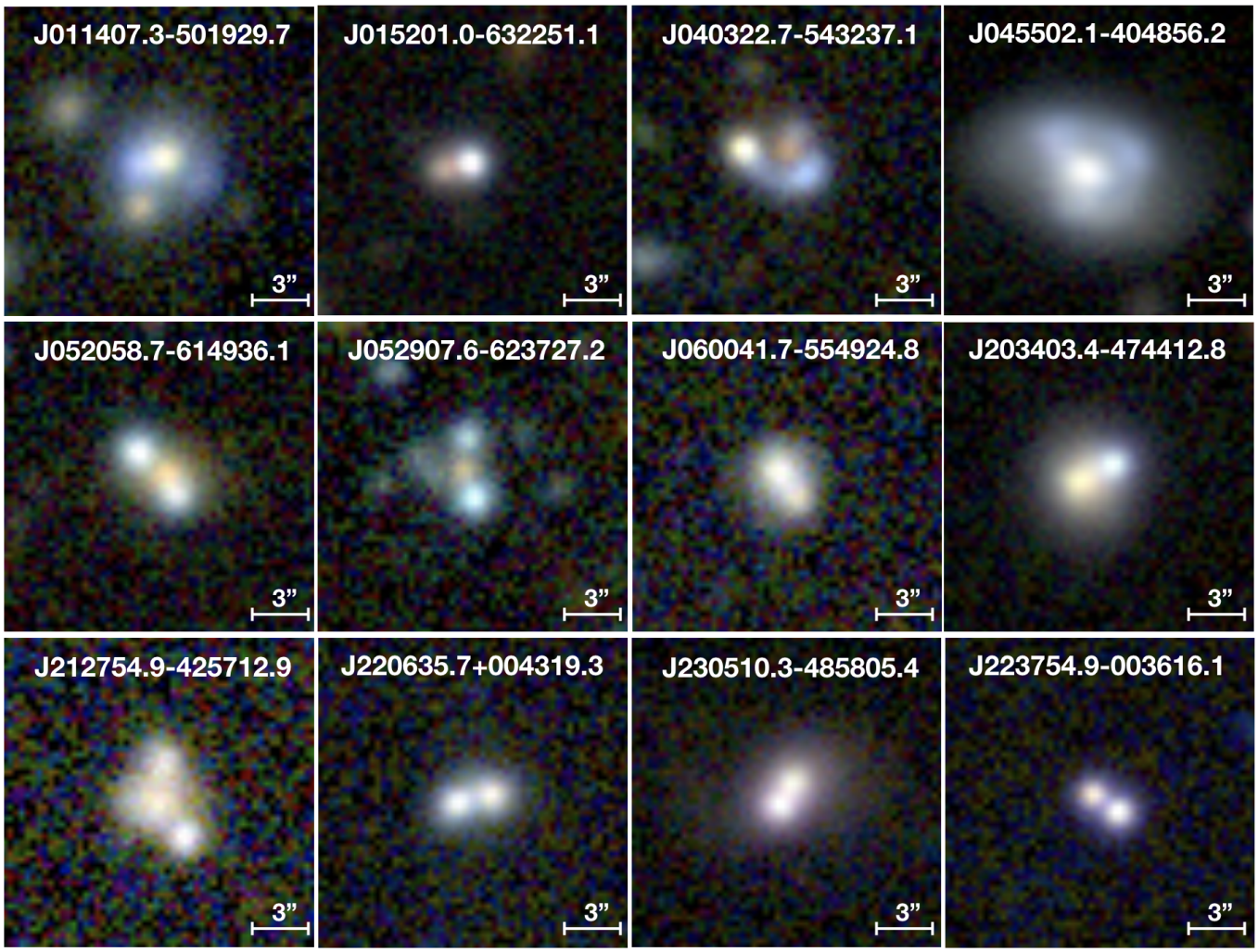


**Fig. 8.** Examples of gravitational lens candidates found through field-corrected offsets between their DES and VISTA coordinates.

containing 198 608 360 objects having good photometry in at least one VISTA band;
- We required a close match with the AllWISE Source catalogue (Cutri et al. 2013) to avoid as many spurious detections as possible and also to cover the mid-infrared bands at 3.4 $\mu$m and 4.6 $\mu$m;
- We cross-matched the VEXAS final table with three of the most used optical wide-sky photometric surveys (the DES, PanSTARRS1, SkyMapper), two X-ray surveys (the ROSAT All Sky Survey, and the *XMM-Newton* Serendipitous Survey), and a 21 cm survey (SUMSS, Bock et al. 1999);
- We cross-matched the VISTA final table with two state-of-the-art spectroscopic surveys, the Sloan Digital Sky Survey (SDSS, DR14, Abolfathi et al. 2018) and the 6dF Galaxy Survey (6dFGS, Jones et al. 2004) to provide test sets for object classification and photometric redshift estimation.
- We showed the scientific potential of the VEXAS cross-matched tables, presenting two extragalactic science cases to search for rare objects in the sky (namely strong gravitational lenses and extremely red objects).

The extension of near-IR catalogue tables (from VISTA) to magnitudes in other wavebands enhances the purity and completeness of object classification, ensuring wide and homogeneous investigation into galaxies, stars, quasars, and peculiar objects. The depth of VISTA naturally extends the scientific scope of research that relied on shallower magnitudes, for example from 2MASS, and the cross-match with optical surveys enables a first characterisation of objects with extreme SEDs.

This first release included only catalogue cross-matches and was restricted to the SGH ($b < -20$ deg). The only space-based mission included here is WISE, thanks to its all-sky coverage and fair depth. This release does not include regions that strongly overlap with the Galactic disc ($-20\,\mathrm{deg} < b < 200\,\mathrm{deg}$), which were already processed to a more advanced stage through the VVV survey (Minniti et al. 2010).

While the current VEXAS catalogue tables are already beyond the state of the art, they can be further developed for subsequent releases. First, the same procedures can be extended to the northern Galactic hemisphere region ($b > 20$ deg, Dec $< 0$). Second, additional information can be added through near-UV and far-UV detections in GALEX, which we chose not to include here due to its rather shallow limits especially for extragalactic objects. Third, increased spatial resolution can be obtained through the ESA-*Gaia* (Gaia Collaboration 2018) and *Hubble* Source Catalog (Whitmore et al. 2016). In this first release, we preferred not to include *Gaia* and *Hubble* Space Telescope (HST) cross-matches for two main reasons: the HST catalogue has sparse waveband and positional coverage; and the *Gaia* catalogue completeness towards fainter magnitudes or small object-separations is currently poor. Dedicated cross-matching with *Gaia* and HST, as ancillary tables, will be part of future releases.

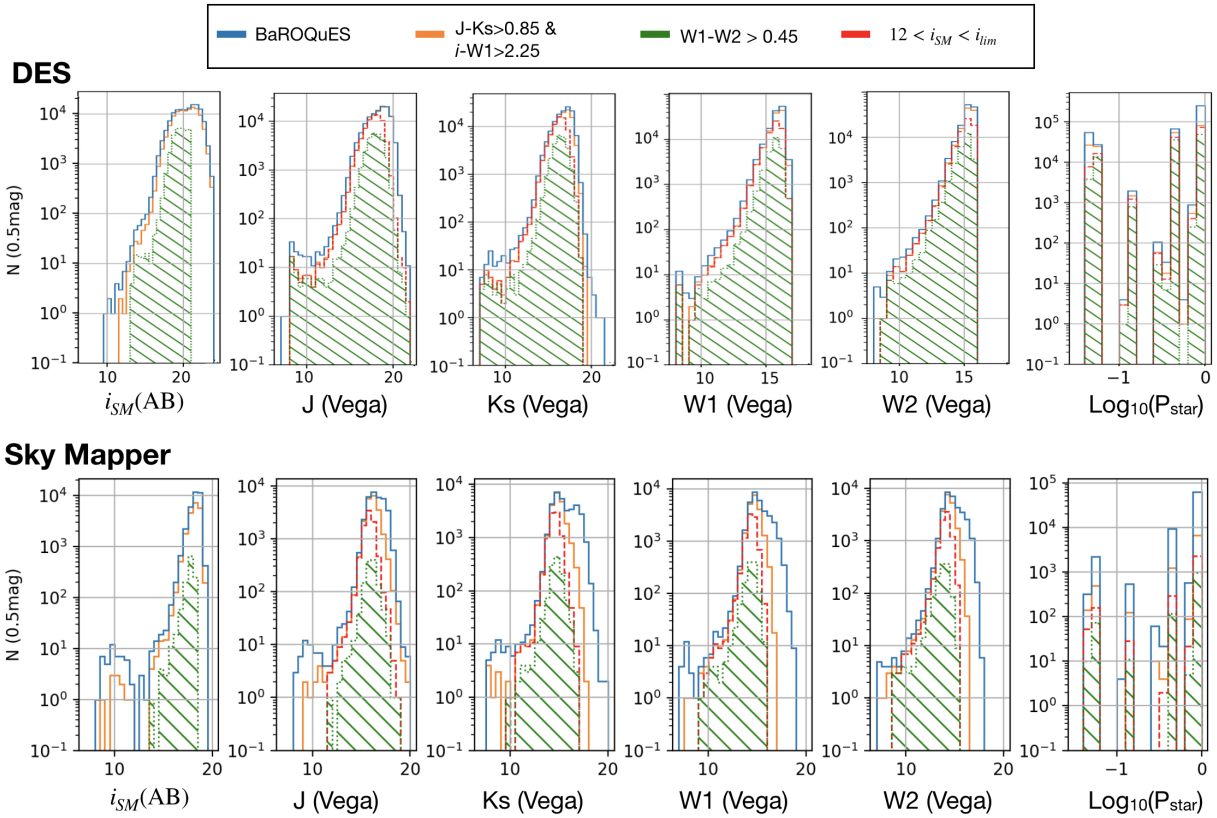


**Fig. 9.** Histograms of magnitudes and stellarity of objects with anomalous astrometric offsets in DES (*top row*), and in SkyMapper with Dec < −70 (*bottom row*). Different nested histograms correspond to incremental cuts in hybrid colours and limiting magnitude, and to a strict extragalactic cut in WISE. The limiting $i$-band magnitude is chosen as $i_{\rm lim} = 21$ for DES, corresponding to current limits for spectroscopic follow-up on ≈4 m class telescopes, and $i_{\rm lim} = 19$ for SkyMapper, simply as the limiting depth of its DR1. WISE preselection is not a limiting factor for wide and shallow searches ($i \lesssim 19$), but it does become the main limitation in deeper searches ($i \lesssim 21$).

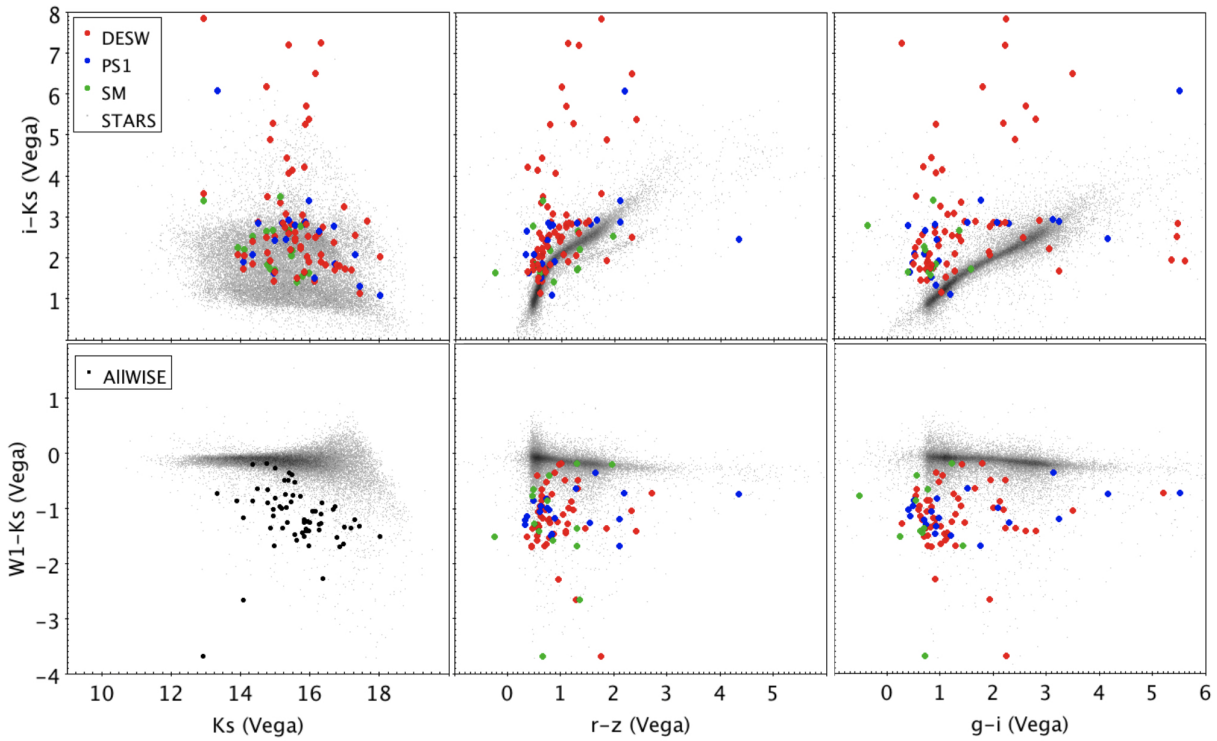


**Fig. 10.** Known lenses from the literature in colour–magnitude and colour–colour multi-wavelength plots. Different colour-coding identifies lenses recovered in different VEXAS sub-tables, as explained in the captions. Small grey points are objects with a spectroscopic match and class=STARS

*Acknowledgements.* CS has received funding from the European Union's Horizon 2020 research and innovation programme under the Marie Skłodowska-Curie actions grant agreement No 664931. AA is supported by a grant from VILLUM FONDEN (project number 16599). This project is funded by the Danish council for independent research under the project "Fundamentals of Dark Matter Structures", DFF – 6108-00470. Based on observations obtained as part of the VISTA Hemisphere Survey, ESO Progamme, 179.A-2010 (PI: McMahon). This publication has made use of data from the VIKING survey from VISTA at the ESO Paranal Observatory, programme ID 179.A-2004. Data processing has been contributed by the VISTA Data Flow System at CASU, Cambridge, and WFAU, Edinburgh. This project used public optical archival data from the Dark Energy Survey (DES), the SkyMapper Southern Sky Survey (SM), the Panoramic Survey Telescope & Rapid Response System DR1 (PanSTARRS1), Sloan Digital Sky Survey IV (SDSS DR14), and the 6dF Galaxy Survey (6dFGS). This publication also makes use of data products from the Wide-field Infrared Survey Explorer, which is a joint project of the University of California, Los Angeles, and the Jet Propulsion Laboratory/California Institute of Technology, funded by the National Aeronautics and Space Administration. This research has made use of the SIMBAD database, operated at CDS, Strasbourg, France; the VizieR catalogue access tool, CDS, Strasbourg, France (DOI: 10.26093/cds/vizier); the NASA/IPAC Infrared Science Archive, operated by the Jet Propulsion Laboratory, California Institute of Technology, under contract with the National Aeronautics and Space Administration; and the NOAO Data Lab. NOAO is operated by the Association of Universities for Research in Astronomy (AURA), Inc., under a cooperative agreement with the National Science Foundation.

## References


Abbott, T. M. C., Abdalla, F. B., Allam, S., et al. 2018, ApJS, 239, 18
Abolfathi, B., Aguado, D. S., Aguilar, G., et al. 2018, ApJS, 235, 42
Agnello, A., & Spiniello, C. 2019, MNRAS, 2132
Agnello, A., Treu, T., Ostrovski, F., et al. 2015, MNRAS, 454, 1260
Agnello, A., Schechter, P. L., Morgan, N. D., et al. 2018a, MNRAS, 475, 2086
Agnello, A., Lin, H., Kuropatkin, N., et al. 2018b, MNRAS, 479, 4345
Andreani, P., Cimatti, A., Loinard, L., et al. 2000, A&A, 354, L1
Anguita, T., Schechter, P. L., Kuropatkin, N., et al. 2018, MNRAS, 480, 5017
Assef, R. J., Stern, D., Kochanek, C. S., et al. 2013, ApJ, 772, 26
Bañados, E., Venemans, B. P., Decarli, R., et al. 2016, ApJS, 227, 11
Bochanski, J. J., Munn, J. A., Hawley, S. L., et al. 2007, AJ, 134, 2418
Bock, D. C.-J., Large, M. I., & Sadler, E. M. 1999, AJ, 117, 1578
Boller, T., Freyberg, M., & Truemper, J. 2014, The X-ray Universe, 2014, 40
Boller, T., Freyberg, M. J., Trümper, J., et al. 2016, A&A, 588, A103
Bonifacio, P., Monai, S., & Beers, T. C. 2000, AJ, 120, 2065
Brown, M. J. I., Jannuzi, B. T., Dey, A., & Tiede, G. P. 2005, ApJ, 621, 41
Carnall, A. C., Shanks, T., Chehade, B., et al. 2015, MNRAS, 451, L16
Carnero Rosell, A., Santiago, B., dal Ponte, M., et al. 2019, MNRAS, 489, 5301
Cassata, P., Cimatti, A., Kurk, J., et al. 2008, A&A, 483, L39
Chambers, K. C., Magnier, E. A., Metcalfe, N., et al. 2016, ArXiv e-prints [arXiv:1612.05560]
Chehade, B., Carnall, A. C., Shanks, T., et al. 2018, MNRAS, 478, 1649
Cross, N. J. G., Collins, R. S., Mann, R. G., et al. 2012, A&A, 548, A119
Cutri, R. M., Wright, E. L., Conrow, T., et al. 2013, VizieR Online Data Catalog: II/328
Daddi, E., Cimatti, A., & Renzini, A. 2000, A&A, 362, L45
Dark Energy Survey Collaboration (Abbott, T., et al.) 2016, MNRAS, 460, 1270
Diehl, H. T., & Dark Energy Survey Collaboration 2012, Phys. Proc., 37, 1332
Driver, S. P., Hill, D. T., Kelvin, L. S., et al. 2011, MNRAS, 413, 971
Drlica-Wagner, A., Bechtol, K., Rykoff, E. S., et al. 2015, ApJ, 813, 109
Dwelly, T., Salvato, M., Merloni, A., et al. 2017, MNRAS, 469, 1065
Edge, A., Sutherland, W., Kuijken, K., et al. 2013, The Messenger, 154, 32
Elston, R., Rieke, G. H., & Rieke, M. J. 1988, ApJ, 331, L77
Emerson, J., McPherson, A., & Sutherland, W. 2006, The Messenger, 126, 41
Gaia Collaboration (Prusti, T., et al.) 2016, A&A, 595, A1
Gaia Collaboration (Brown, A. G. A., et al.) 2018, A&A, 616, A1
Gilmore, G., Randich, S., Asplund, M., et al. 2012, The Messenger, 147, 25
González-Fernández, C., Hodgkin, S. T., Irwin, M. J., et al. 2018, MNRAS, 474, 5459
Gonzalez-Perez, V., Baugh, C. M., Lacey, C. G., & Kim, J.-W. 2011, MNRAS, 417, 517
Hildebrandt, H., Viola, M., Heymans, C., et al. 2017, MNRAS, 465, 1454
Inada, N., Oguri, M., Shin, M.-S., et al. 2012, AJ, 143, 119
Jones, D. H., Saunders, W., Colless, M., et al. 2004, MNRAS, 355, 747
Jones, D. H., Read, M. A., Saunders, W., et al. 2009, MNRAS, 399, 683
Kaiser, N., Aussel, H., Burke, B. E., et al. 2002, Proc. SPIE, 4836, 154
Kong, X., Daddi, E., Arimoto, N., et al. 2006, ApJ, 638, 72
Khramtsov, V., Sergeyev, A., Spiniello, C., et al. 2019, A&A, submitted [arXiv:1906.01638]
Kuijken, K., Heymans, C., Hildebrandt, H., et al. 2015, MNRAS, 454, 3500
Lemon, C. A., Auger, M. W., McMahon, R. G., et al. 2018, MNRAS, 479, 5060
Liske, J., Baldry, I. K., Driver, S. P., et al. 2015, MNRAS, 452, 2087
Mainzer, A., Bauer, J., Grav, T., et al. 2011, ApJ, 731, 53
Majewski, S. R., Skrutskie, M. F., Weinberg, M. D., et al. 2003, ApJ, 599, 1082
Maturi, M., Bellagamba, F., Radovich, M., et al. 2019, MNRAS, 485, 498
Mauch, T., Murphy, T., Buttery, H. J., et al. 2003, MNRAS, 342, 1117
McCarthy, P. J., Persson, S. E., & West, S. C. 1992, ApJ, 386, 52
McMahon, R. G., Banerji, M., Gonzalez, E., et al. 2013, The Messenger, 154, 35
Minniti, D., Lucas, P. W., Emerson, J. P., et al. 2010, New Astron., 15, 433
Muñoz, J. A., Falco, E. E., Kochanek, C. S., et al. 1998, Ap&SS, 263, 51
Oguri, M., & Marshall, P. J. 2010, MNRAS, 405, 2579
Ostrovski, F., Lemon, C. A., Auger, M. W., et al. 2018, MNRAS, 473, L116
Petrillo, C. E., Tortora, C., Vernardos, G., et al. 2019, MNRAS, 484, 3879
Reed, S. L., McMahon, R. G., Banerji, M., et al. 2015, MNRAS, 454, 3952
Roche, N. D., Almaini, O., Dunlop, J., Ivison, R. J., & Willott, C. J. 2002, MNRAS, 337, 1282
Roy, N., Napolitano, N. R., La Barbera, F., et al. 2018, MNRAS, 480, 1057
Salvato, M., Buchner, J., Budavari, T., et al. 2018, VizieR Online Data Catalog: J/MNRAS/473/4937
Saracco, P., Longhetti, M., Severgnini, P., et al. 2005, MNRAS, 357, L40
Schlegel, D. J., Finkbeiner, D. P., & Davis, M. 1998, ApJ, 500, 525
Scoville, N., Aussel, H., Benson, A., et al. 2007, ApJS, 172, 150
Shanks, T., Metcalfe, N., Chehade, B., et al. 2015, MNRAS, 451, 4238
Shin, J., Shim, H., Hwang, H. S., et al. 2017, J. Korean Astron. Soc., 50, 61
Shipp, N., Drlica-Wagner, A., Balbinot, E., et al. 2018, ApJ, 862, 114
Skrutskie, M. F., Cutri, R. M., Stiening, R., et al. 2006, AJ, 131, 1163
Spiniello, C., Agnello, A., Napolitano, N. R., et al. 2018, MNRAS, 480, 1163
Spiniello, C., Sergeyev, A. V., Marchetti, L., et al. 2019a, MNRAS, 485, 5086
Spiniello, C., Agnello, A., Sergeyev, A. V., et al. 2019b, MNRAS, 483, 3888
Stiavelli, M., Treu, T., Carollo, C. M., et al. 1999, A&A, 343, L25
Sutherland, W. 2012, Science from the Next Generation Imaging and Spectroscopic Surveys, 40
Taylor, M. B. 2005, Astron. Data Anal. Soft. Syst. XIV, 347, 29
Thompson, D., Beckwith, S. V. W., Fockenbrock, R., et al. 1999, ApJ, 523, 100
Tonry, J. L., Stubbs, C. W., Lykke, K. R., et al. 2012a, ApJ, 750, 99
Tonry, J. L., Stubbs, C. W., Kilic, M., et al. 2012b, ApJ, 745, 42
Truemper, J. 1982, Adv. Space Res., 2, 241
Venemans, B. P., Findlay, J. R., Sutherland, W. J., et al. 2013, ApJ, 779, 24
Venemans, B. P., Verdoes Kleijn, G. A., Mwebaze, J., et al. 2015, MNRAS, 453, 2259
Vikram, V., Chang, C., Jain, B., et al. 2015, Phys. Rev. D, 92, 022006
Voges, W., Aschenbach, B., Boller, T., et al. 1999, A&A, 349, 389
Voges, W., Aschenbach, B., Boller, T., et al. 2000, IAU Circ., 7432, 3
Watson, M. G., Auguères, J.-L., Ballet, J., et al. 2001, A&A, 365, L51
Whitmore, B. C., Allam, S. S., Budavári, T., et al. 2016, AJ, 151, 134
Wright, E. L., Eisenhardt, P. R. M., Mainzer, A. K., et al. 2010, AJ, 140, 1868
Wolf, C., Bian, F., Onken, C. A., et al. 2018, PASA, 35, e024